Chaos, Solitons and Fractals 178 (2024) 114331

Contents lists available at ScienceDirect

Chaos, Solitons and Fractals

journal homepage: www.elsevier.com/locate/chaos

Statistical mechanical characterization of billiard systems

Kivanc Cetin [a,*], Ugur Tirnakli [b], Diego F.M. Oliveira [c], Edson D. Leonel [d]

[a] American Collegiate Institute, Izmir, 35290, Turkey
[b] Department of Physics, Faculty of Arts and Sciences, Izmir University of Economics, Izmir, 35330, Turkey
[c] School of Electrical Engineering and Computer Science - University of North Dakota, Grand Forks, ND, USA
[d] Departamento de Fisica, UNESP-Univ Estadual Paulista, Av.24A, 1515 Bela Vista, Rio Claro, 13506-900, SP, Brazil

ARTICLE INFO

Keywords:
Billiard systems
Nonlinear dynamics
Nonextensive statistical mechanics

ABSTRACT

Area-preserving maps play an important role in diverse fields as they are widely used for modeling complex systems. In addition, these maps provide rich observations by presenting stable orbits and chaotic behavior separately or together in the phase space depending on the control parameter. In recent years, several studies on these maps, drawing inspiration from the phase space dynamics, have shown that nonextensive statistical mechanics provides appropriate instruments to characterize these systems. In this study, we perform a rigorous numerical analysis to delve into the statistical mechanical properties of a billiard system. Our primary goal is to confirm the presence of a q-Gaussian distribution, with an estimated q value of approximately 1.935. We accomplish this by examining the probability distribution of the cumulative sum of system iterates, focusing specifically on initial conditions within the stability islands. Our findings align seamlessly with the latest research in this field. Furthermore, we show that a multi-component probability distribution containing both Gaussian and q-Gaussians describes the entire system for some parameter regions where the phase space consists of stability islands together with the chaotic sea.

1. Introduction

Several studies demonstrating the use of non-extensive statistical mechanics in dynamical systems have been carried out in recent years, and connections among diverse systems and disciplines have been enlightened [1,2]. The framework of this formalism explains the limiting behavior of systems that have a correlated nature and are neither ergodic nor mixing, where the Boltzmann–Gibbs (BG) statistical mechanics do not apply. While the BG approach succeeds in describing the long-term behavior of ergodic and mixing systems with a positive largest Lyapunov exponent (LLE), i.e., systems in a strongly chaotic regime, nonextensive statistical mechanics, which includes the BG mechanics as a particular case, can describe the long-term behavior of nonergodic systems with zero (or numerically almost zero) LLE. As the q-Gaussian distribution is one of the pillars of nonextensive statistical mechanics, numerical and analytical methods have been used to verify the existence of this distribution, which includes the Gaussian case in the limit of $q \to 1$. A large number of studies in the literature have shown that the limiting probability distributions of systems in strongly chaotic regimes and weakly chaotic regimes evolve on a Gaussian and a q-Gaussian, respectively [3–9]. For area-preserving maps such as the standard, the Web, and the Harper maps, in all previous numerical works, it has been observed that the limiting distribution of the conditions located inside the stability islands, where the system is not ergodic and mixing, and trajectories exhibit a strongly correlated nature, approach a q-Gaussian with a specific $q \simeq 1.935$ value which is considered to be universal behavior for all members of this map family [7,8,10]. On the other hand, recent analytical work on the standard map with the specific parameter case which makes the system integrable [9] showed that the asymptotic value of q parameter approaches $q = 2$, which makes the governing distribution to become the Cauchy distribution. Finally, it is worth noting that recent studies on two generalizations of the standard map presented that the sticky behavior occurring in the strongly chaotic sea meets the conditions of the occurrence of the q-Gaussian family by exhibiting the lack of mixing and relatively strongly correlated nature, and the observation of q-Gaussian limiting distribution for this behavior confirms the robustness [10,11].

This paper investigates some statistical properties of an area-preserving elliptical–oval billiard model. Billiards are dynamic systems in which a point particle travels and experiences collisions with a closed region. Mathematically, a billiard is defined by a connected region $Q \subset R^D$, with boundary $\partial Q \subset R^{D-1}$ which separates Q from its complement. If the set ∂Q is constant concerning time, the

* Corresponding author.
E-mail addresses: kivanccetin@hotmail.com (K. Cetin), ugur.tirnakli@ieu.edu.tr (U. Tirnakli), diegofregolente@gmail.com (D.F.M. Oliveira), edson-denis.leonel@unesp.br (E.D. Leonel).

https://doi.org/10.1016/j.chaos.2023.114331
Received 27 September 2023; Received in revised form 22 November 2023; Accepted 28 November 2023
Available online 14 December 2023

particle does not change its energy upon collision with the boundary. It is significant to highlight that three essential control parameters meticulously govern the boundary configuration. By skillfully manipulating these parameters, a comprehensive spectrum of outcomes can be achieved, from the well-studied circular [12] and elliptical billiards [13] to the more intricate oval billiard scenarios [14]. Moreover, by simultaneously manipulating two control parameters, an entirely novel realm of possibilities is unveiled, culminating in the creation of an elliptical–oval billiard geometry. Within this closed boundary, a classical particle of mass m travels without being affected by any external field. Upon collision with the border, the particle exhibits specular reflection without undergoing any fractional energy loss. The intriguing phase space of the system showcases a blend of order and chaos. Depending on the combination of control parameters and initial conditions, we observe the emergence of KAM (Kolmogorov–Arnold–Moser) islands, encircled by a chaotic sea, all bounded by sets of invariant spanning curves [15–17]. Interestingly, depending on the combination of the control parameters, regions on the boundary exhibit a transition from positive to negative curvature. Once this change occurs, all the invariant spanning curves are destroyed. This model is essential from the point of view of our purpose here by exhibiting ergodic and nonergodic behaviors in the available phase space, tuning the control parameters. It also provides a benchmark in the field of chaos theory.

Billiard systems play a pivotal role in scientific research and experimentation. Their deference to both analytical and numerical investigations has enabled comprehensive explorations of various facets, encompassing chaotic dynamics [18,19], diffusion and particle transport [20,21], the semiclassical limit [22], as well as energy absorption and dissipation. Fermi pioneered the latter aspect as an endeavor to try to understand the origins of cosmic ray acceleration [23,24]. Subsequently, this approach has proven valuable in diverse fields, such as nuclear physics, plasma physics, and astrophysics [25–27]. Recently, researchers achieved geometric confinement with atomically precise shapes resembling lattice billiards by utilizing laser-induced quenches on a TaS2 material [28].

In this study, in a similar fashion to other area-preserving maps (e.g., the standard map and its two generalizations [6,10,11]), we select control parameters to provide phase spaces with different stability island and chaotic sea occupancy ratios. For each parameter set, the dynamics and LLE characterizations of the phase spaces are analyzed by choosing random initial conditions from the entire phase space. The limiting distributions are then computed numerically using many initial conditions that are iterated over long time steps.

2. The billiard model

This section addresses the intricacies of constructing a nonlinear mapping that describes the dynamics of a two-dimensional billiard. We describe the dynamics exhibited by a classical particle characterized by mass m, confined within a bounded domain that engenders elastic, specular collisions with its enclosing perimeter. Upon impact with the boundary, the particle undergoes an elastic reflection, retaining its initial velocity. When we represent the dimensions of the border using polar coordinates, the resulting formulation is as follows:

$$R(\theta, p, e, \epsilon) = \left[\frac{1-e^2}{1+e\cos(\theta)}\right] + \epsilon\cos(p\theta)\ . \tag{1}$$

Here, the control parameter $e \in [0, 1)$ dictates the degree of circle deformation, thereby enabling the recovery of circular and elliptical shapes. Concurrently, the control parameter $\epsilon \in [0, 1)$ exercises influence over circle deformation, facilitating the realization of oval configurations. The integer value p and angular parameter $\theta \in [0, 2\pi)$, denoting a counterclockwise angle concerning the positive horizontal axis, complete this framework. By setting $e = \epsilon = 0$, we revisit the domain with a circular boundary. In instances where $e \neq 0$ and $\epsilon = 0$, an elliptical edge manifests. The border is oval for scenarios featuring $e = 0$ alongside $\epsilon \neq 0$. An elliptical oval-like boundary configuration emerges when $e \neq 0$ and $\epsilon \neq 0$. This meticulous examination of varying parameter configurations augments our comprehension of the boundary's influence on particle dynamics.

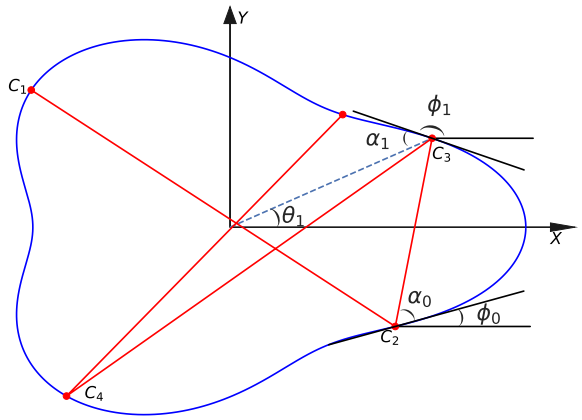

Fig. 1. Illustration of the model.

Following the established norms of scientific literature, the particle's dynamics are expounded through a two-dimensional nonlinear mapping, symbolized as $T(\theta_n, \alpha_n) = (\theta_{n+1}, \alpha_{n+1})$, in a manner that is traditional within the field. Within this context, the dynamic variable θ_n signifies the angular position of the particle at the point of contact with the boundary. At the same time, α_n represents the angle formed by the trajectory and the tangent vector corresponding to the boundary's angular position θ_n (as depicted in Fig. 1). The subscript n designates the particle's nth collision with the boundary. By using polar coordinates, we can derive expressions for both $X(\theta_n)$ and $Y(\theta_n)$ in the following manner:

$$X(\theta_n) = \left[\frac{1-e^2}{1+e\cos(\theta_n)} + \epsilon\cos(p\theta_n)\right]\cos(\theta_n)\ , \tag{2}$$

$$Y(\theta_n) = \left[\frac{1-e^2}{1+e\cos(\theta_n)} + \epsilon\cos(p\theta_n)\right]\sin(\theta_n)\ . \tag{3}$$

Given an initial condition of (θ_n, α_n), the angle between the tangent and the abscissa at the position $X(\theta_n)$ and $Y(\theta_n)$ is defined as:

$$\phi_n = \arctan\left[\frac{Y'(\theta_n)}{X'(\theta_n)}\right], \tag{4}$$

with the expressions for $X'(\theta_n)$ and $Y'(\theta_n)$ being:

$$X'(\theta_n) = \frac{dR(\theta_n)}{d\theta_n}\cos(\theta_n) - R(\theta_n)\sin(\theta_n)\ , \tag{5}$$

$$Y'(\theta_n) = \frac{dR(\theta_n)}{d\theta_n}\sin(\theta_n) + R(\theta_n)\cos(\theta_n)\ . \tag{6}$$

The term $\frac{dR(\theta_n)}{d\theta_n}$ is given by:

$$\frac{dR(\theta_n)}{d\theta_n} = \frac{(1-e^2)e\sin(\theta_n)}{[1+e\cos(\theta_n)]^2} - \epsilon p\sin(p\theta_n). \tag{7}$$

It is crucial to underscore that the particle remains unaffected by any external field during its interactions with the boundary. Consequently, the particle maintains a constant velocity along a straight trajectory until it encounters the boundary. To ascertain the particle's new angular position upon its subsequent collision with the border, the ensuing equation must be solved:

$$Y(\theta_{n+1}) - Y(\theta_n) = \tan(\alpha_n + \phi_n)[X(\theta_{n+1}) - X(\theta_n)]. \tag{8}$$

Here, ϕ_n is derived from the slope between the tangent vector and the positive horizontal axis. The new positions of the particle at angular

position θ_{n+1}, denoted as $X(\theta_{n+1})$ and $Y(\theta_{n+1})$, are numerically determined solutions of Eq. (8). The subsequent angle, α_{n+1}, representing the trajectory's orientation concerning the tangent at θ_{n+1}, is deduced from geometric considerations, as illustrated in Fig. 1, and is expressed as:

$$\alpha_{n+1} = \phi_{n+1} - (\alpha_n + \phi_n). \tag{9}$$

The geometric configuration in Fig. 1 provides insight into determining the new angle α_{n+1}. Accordingly, the model's dynamics are characterized by the following map:

$$T : \begin{cases} F(\theta_{n+1}) = R(\theta_{n+1})\sin(\theta_{n+1}) - Y(\theta_n) - \tan(\alpha_n + \phi_n) \\ \quad \times [R(\theta_{n+1})\cos(\theta_{n+1}) - X(\theta_n)] \\ \alpha_{n+1} = \phi_{n+1} - (\alpha_n + \phi_n) \end{cases}, \tag{10}$$

where θ_{n+1} is determined numerically as the solution to $F(\theta_{n+1}) = 0$. Here one can calculate $R(\theta_{n+1})$ and ϕ_{n+1} from Eqs. (1) and (4) respectively, changing $\theta \to \theta_{n+1}$ and $\phi_n \to \phi_{n+1}$.

The analyses use $e = 0$ and $\epsilon \neq 0$ conditions to obtain chaotic sea in the systems. To reduce the time requirement of the numerical calculations containing a root-finding process, the condition $\epsilon < \epsilon_c$ is focused on, where

$$\epsilon_c = \frac{1}{1+p^2}, \quad p \geq 1. \tag{11}$$

As mentioned earlier, it is important to note that the condition corresponds to the convex boundary formation explained in detail in [29–31].

We numerically investigate the phase space dynamics and limiting distributions of the billiard systems with $p = 1$, for $\epsilon = 0$, $\epsilon = 0.2$, $\epsilon = 0.25$, and $\epsilon = 0.49$ parameter values. The $\epsilon = 0$ and $\epsilon = 0.49$ cases are selected to provide extreme scenarios in which the stability islands and the chaotic sea fully occupy the phase spaces, respectively. Even though few stability islands can still exist in the $\epsilon = 0.49$ case, they occupy a tiny region in the phase space as given in Fig. 2 and can be considered statistically negligible. Between these two extremes, the chaotic sea covers a more extensive region with increasing ϵ value, and the changes in the phase space dynamics and limiting distributions can be compared. The findings are depicted in Fig. 2 in order to enhance the visualization of the system's temporal progression. To show how the trajectory behavior changes in the phase space according to the increase of the ϵ term, for each scenario, we iterate the system $T = 10^3$ times, starting from $M = 100$ initial conditions randomly chosen over the whole phase space. The obtained phase space portraits are given in the first column of Fig. 2.

2.1. Quantification of the phase space behavior: Lyapunov exponent analysis

To quantify the qualitative observation made for the trajectory behavior in the phase space portraits, the Benettin algorithm [32] is used to calculate the LLE (λ) which is defined as

$$\lambda = \frac{1}{T}\sum_{i=1}^{T} \ln\left(\frac{d(i)}{\sqrt{2}\,\Delta_\theta^{(0)}}\right), \tag{12}$$

where T is the iteration time and $d(i) = \left[(\Delta_\theta^{(i)})^2 + (\Delta_\alpha^{(i)})^2\right]^{1/2}$ is the Euclidean distance at time i in the phase space between initially neighboring trajectories. For each $M = 2 \times 10^6$ initial conditions randomly chosen from the whole phase space, the LLE is computed separately for all cases using $T = 5 \times 10^5$ iteration steps. The initial distance between a randomly chosen initial condition and its neighbor is set to $\Delta_\alpha^{(0)} = \Delta_\theta^{(0)} = 10^{-8}$. To quantify the trajectory behavior in the phase space portrait, the calculated magnitudes of the LLE are represented by color maps, which are given in the second column of Fig. 2. This method is similar, but not the same, as previously used in the literature, known as the finite-time Lyapunov exponent [33–36]. The calculated LLE values are nearly zero ($\lambda \approx 0$) for initial conditions within the stability islands, while they are largely positive for the chaotic trajectories. The stability islands are said to be in a weakly chaotic regime, consistent with their LLE magnitudes [6]. Since the system in the strongly chaotic and weakly chaotic regimes is ergodic and nonergodic, it becomes possible to distinguish regions of different behavior in the phase space. In addition, phase space occupation ratios of these different behavior regions can be determined from LLE spectra.

3. Statistical mechanical characterization of the model

Since the ergodic and nonergodic behaviors can occur separately and together in the phase space depending on the ϵ parameter value, the limiting distributions of the above scenarios are analyzed by staying within the Central Limit Theorem (CLT) framework. In accordance with the previous studies [3–8], the variable

$$y = \frac{1}{\sqrt{T}}\sum_{i=1}^{T}(\theta_i - \langle\theta\rangle) \tag{13}$$

is defined, where T is the number of iterations. In Eq. (13), $\langle\dots\rangle$ denotes both time average over T iterations and ensemble average over M chosen initial conditions, i.e.,

$$\langle\theta\rangle = \frac{1}{M}\frac{1}{T}\sum_{l=1}^{M}\sum_{i=1}^{T}\theta_i^{(l)}. \tag{14}$$

The probability distributions are obtained as independent from the number of iterations used in the numerical calculations by defining the variable y following the CLT. It was recently shown for weakly chaotic regimes of several dissipative [3,4] and area-preserving maps [6–8,10,11] that, limiting distributions of the sum of iterates of the map given in Eq. (13) seem to approach a q-Gaussian form which can be defined as

$$P_q(y;\mu_q,\sigma_q) = A_q\sqrt{B_q}[1-(1-q)B_q(y-\mu_q)^2]^{\frac{1}{(1-q)}} \tag{15}$$

where A_q is normalization factor, B_q is the parameter which characterizes the width of the distribution, μ_q is q-mean value and σ_q is q-variance [37]:

$$A_q = \begin{cases} \dfrac{\Gamma\left[\frac{5-3q}{2(1-q)}\right]}{\Gamma\left[\frac{2-q}{1-q}\right]}\sqrt{\dfrac{1-q}{\pi}}, & q < 1 \\ \dfrac{1}{\sqrt{\pi}}, & q = 1 \\ \dfrac{\Gamma\left[\frac{1}{q-1}\right]}{\Gamma\left[\frac{3-q}{2(q-1)}\right]}\sqrt{\dfrac{q-1}{\pi}}, & 1 < q < 3 \end{cases} \tag{16}$$

$$B_q = [(3-q)\sigma_q^2]^{-1}. \tag{17}$$

In Eq. (15), the $q \to 1$ limit corresponds to a Gaussian distribution. Thus, this equation can model the limiting distributions of both ergodic and nonergodic behaviors.

In our analyses, the limiting distributions of the variable y for each case are obtained using 5×10^6 randomly chosen initial conditions, each iterated 2^{22} times. These values of the parameters are carefully chosen to ensure statistical characterization of such area-preserving maps as computational time efficiency is considered. This guarantees the reliability and accuracy of our analyses. The results are shown in the third column of Fig. 2 with the corresponding phase space portraits and the LLE spectra to relate the phase space dynamics to the probability distributions. The parameters related to the limiting distributions (Eq. (15)) of all scenarios are given in Table 1. As seen in Fig. 2, the stability islands with almost zero LLE occupy the entire phase space for $\epsilon = 0$ case, and the limiting distribution of this nonergodic system exhibits a clear q-Gaussian with $q \simeq 1.935$. On the other hand,

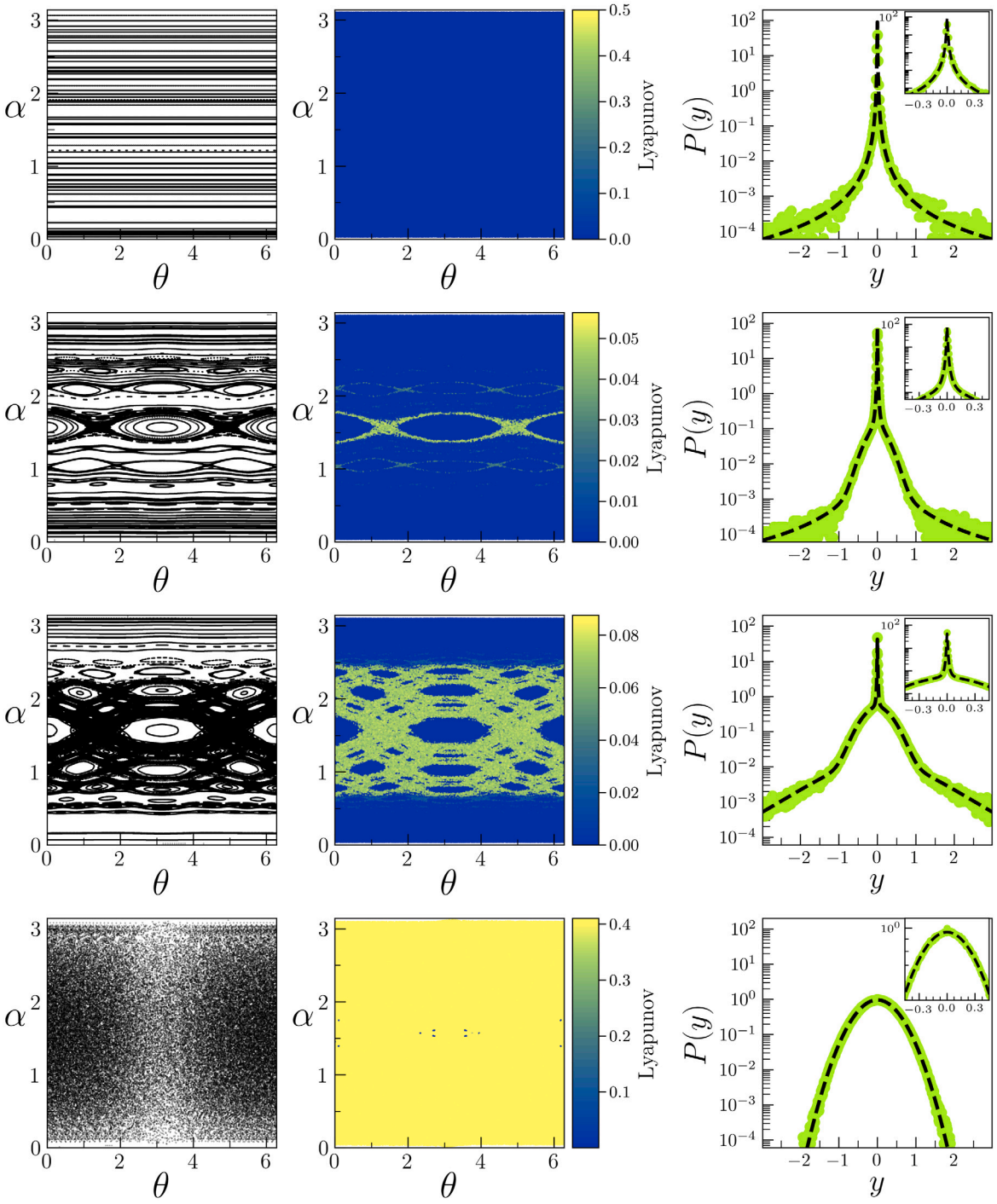

Fig. 2. Analyses of the aforementioned billiard systems. The first, second, third, and fourth rows are for $\epsilon = 0$, $\epsilon = 0.2$, $\epsilon = 0.25$ and $\epsilon = 0.49$ cases, respectively. For all cases, we fix the other parameter as $p = 1$. *Left column:* Phase space portraits, *Middle column:* LLE color map descriptions of the phase portraits, *Right column:* Probability distributions obtained from the initial conditions chosen from the entire phase space. Chaotic behavior dominates larger phase space areas with increasing ϵ. Probability distributions describing the whole system, which consists of different behavior regions with different phase space occupation ratios for each case, evolve on a linear combination of q-Gaussian functions with different q values. (For interpretation of the references to color in this figure legend, the reader is referred to the web version of this article.)

for the $\epsilon = 0.49$ case, the whole phase space is dominated by the chaotic sea with a largely positive LLE, and the system is ergodic and mixing. As expected, the obtained limiting distribution develops on a Gaussian, corresponding to $q \to 1$ limit in Eq. (15). To avoid confusion, for all cases, the probability distribution characterizing the whole space is modeled as a linear combination of $P(y)$ distributions, compatible with the different regimes observed in the phase spaces of the parameter sets, and is given by

$$P(y) = c_{q_1} P_{q_1}(y; \mu_{q_1}, \sigma_{q_1}) + c_{q_2} P_{q_2}(y; \mu_{q_2}, \sigma_{q_2}) + c_{q_3} P_{q_3}(y; \mu_{q_3}, \sigma_{q_3}) \tag{18}$$

where q is the index of a probability distribution emerging from a specific region, c_q is the contribution ratio of P_q function to the limiting distribution of the whole system. In Table 1, the parameters related to Eq. (18) are given together with that of the probability distributions.

Table 1
The obtained parameter values of the probability distributions for all billiard systems given in Fig. 2.

$A_{q=1.935} = 0.3364\ldots$, $A_{q=1.25} = 0.5093\ldots$, $A_{q=1} = 0.5642\ldots$

	$p=1, \epsilon=0$	$p=1, \epsilon=0.2$	$p=1, \epsilon=0.25$	$p=1, \epsilon=0.49$
q_1	1.935	1.935	1.935	1.935
q_2	1	1	1	1
q_3	1	1	1.25	1
c_{q_1}	1	0.95	0.580	0
c_{q_2}	0	0.05	0.386	1
c_{q_3}	0	0	0.034	0
B_{q_1}	71×10^3	54×10^3	45×10^3	0
B_{q_2}	0	7.81	4.48	2.91
B_{q_3}	0	0	0.58	0

Thus, for the $\epsilon = 0$ case, $q_1 \simeq 1.935$, for the $\epsilon = 0.49$ case, $q_1 = 1$ and for both of them $c_{q_1} = 1$. The reason for the use of a three-component distribution function is explained in the following.

With the increment of the ϵ control parameter, the stability islands dissolve according to the Poincaré–Birkhoff Theorem [38] and the KAM Theorem [39] and the chaotic regime develops and occupies larger areas in the phase space. As a result, the chaotic regime and the stability islands, i.e., ergodic and nonergodic behavior, coexist in the phase space for the $\epsilon = 0.2$ and $\epsilon = 0.25$ parameters. Upon analyzing the LLE color map for the $\epsilon = 0.2$ case, it is observed that the stability islands exhibit LLE values within the range of $\lambda \leqslant 2.5 \times 10^{-4}$. In contrast, the chaotic seas exhibit considerably higher positive LLE values. Using the LLE ranges, the separation of different behavior portions in the phase space is achieved, and the phase space occupation ratios of the chaotic regime and stability islands can be determined accurately. The probability distribution characterizes the whole space, Eq. (18), is obtained as a linear combination of a q-Gaussian function with $q_1 \simeq 1.935$ and a Gaussian function ($q_2 = 1$) and the contribution ratios of these functions, c_{q_1} and c_{q_2}, to the limiting distribution of the whole system are the same as the occupation ratios by indicating the accuracy of the method as mentioned above. Here, for this two-component distribution, $c_{q_1} + c_{q_2} = 1$.

At first glance, it can be thought that the limiting distribution of the $\epsilon = 0.25$ case would be a combination of a Gaussian and a q-Gaussian arising from the initial conditions located in the chaotic sea and the stability islands, respectively, as in the previous case. However, a three-component probability distribution modeled by Eq. (18) is obtained where $q_1 \simeq 1.935$, $q_2 = 1$, $q_3 \simeq 1.25$ and $c_{q_1} + c_{q_2} + c_{q_3} = 1$. It is important to note here that, as in the $\epsilon = 0.2$ scenario, the occupation ratio of the stability islands is determined from the LLE spectrum. It is equal to the contribution ratio of $P_{q_1}(y)$ in Eq. (18). The sticky behavior in the chaotic sea is observed when the phase space dynamics and LLE spectrum are analyzed in more detail. As a result of the strong resonances causing stability islands to dissolve [39], complex tangle structures emerge around the archipelagos, and the trajectories within the tangles, seem to stick to them in the phase space. In Fig. 3a, the LLE heat map obtained by eliminating the stability islands whose LLE range is $\lambda \leqslant 2.5 \times 10^{-4}$ shows only the chaotic sea contributions and different chaotic regions with different LLE values can be distinguished. When the phase space dynamics of the trajectories are analyzed, it is observed that the sticky region mainly develops in the less chaotic regions, which can be considered as small chaotic bands. Chaotic trajectories may pass through the sticky regions several times, covering them for unpredictable periods before or after wandering throughout the strongly chaotic sea with seemingly random behavior. In Fig. 3b, an example of the sticky regions is given by iterating two initial conditions in that chaotic band for 4×10^5 times. As can be seen, the black region sticks to stability islands at the top, and this region is not visited by the red-colored trajectory during that time interval. Meanwhile, the black-colored trajectory does not visit the bottom part of the chaotic band. Though the entire band is an allowed space where the chaotic trajectories are expected to cover randomly, some of these trajectories only visit these two regions for long time steps. It should be noted that if a trajectory is traced for the limit of infinite time, the chaotic band would be fully covered by a single trajectory, as expected. However, it is impossible to reach this limit when considering real-life systems and numerical simulations. It is important to note that the sticky behavior occurs also in the strongly chaotic sea. But in the calculation of Eq. (12), although the Euclidean distances are tiny while the trajectory is in the sticky regions, large distance values originating from the trajectory movement in the chaotic sea repress the contribution of the smaller distance values in the summation of logarithmic functions and result in largely positive LLE [11]. Since the calculation of the Lyapunov exponent aims to characterize the long-term behavior of the trajectory, the Benettin algorithm used in this research is accurate. However, the phase space occupation ratio of the sticky behavior cannot be determined directly from the LLE color map because of the unpredictable phase space dynamics. Due to this, the contribution of the probability distribution arising from the sticky behavior is determined numerically from the obtained probability distribution of the whole system. At this point, it is worth noting that stickiness and the detection of sticky regions have already been the subject of study in the literature [40,41].

Recent studies of the two generalizations of the area-preserving standard map have shown that the trajectories within the sticky regions exhibit a correlated nature and the lack of the mixing property [10,11]. Since two requirements for q-Gaussian distributions to arise in a system are fulfilled by the sticky behavior, a second q-Gaussian function must occur at the limiting distribution in addition to the one with $q \simeq 1.935$ emerging from the initial conditions located inside the stability islands. The q-Gaussian distribution arising from the sticky behavior has a smaller q value than $q \simeq 1.935$ because the trajectories visiting the sticky regions exhibit a weaker correlated nature compared to those in the stability islands [10,11]. In line with previous analyses of the standard map, one can conclude that the q-Gaussian with $q \simeq 1.25$ contribution in the limit distribution of the $\epsilon = 0.25$ case emerges because of the stickiness observed in the phase space. To reinforce this inference, the $p = 2, \epsilon = 0.1$ billiard system exhibiting strong sticky regions has been analyzed and a q-Gaussian with $q \simeq 1.41$ has emerged in the three-component probability distribution together with a Gaussian and a q-Gaussian with $q \simeq 1.935$. However, the presentation of this analysis is intentionally omitted in this paper to maintain the coherence and continuity of the narrative. It is worth mentioning that q-Gaussian distribution originating from the sticky behavior converges to a Gaussian in the infinite time limit where the system would be ergodic. For the present case, to represent the robustness of the Gaussian and q-Gaussian with $q \simeq 1.935$ distributions, initial conditions chosen from the stability islands and the chaotic sea are also analyzed individually, and the results are given in Fig. 4. As the q-Gaussian distribution requires a large number of experiments iterated for long time steps, each of 2×10^6 conditions iterated 2^{22} times and a clear q-Gaussian with $q \simeq 1.935$ is obtained as a limiting distribution. On the contrary, the Gaussian distribution is quickly achieved with 2^{18} iterations applied for 4×10^5 initial conditions having largely positive LLE values. Strictly speaking, the limiting distribution of the whole system and its three components seems to be robust.

4. Conclusion

The billiard systems present complex phase space dynamics and provide rich observations from the statistical mechanical point of view. For all cases presenting stability islands in the phase space, a q-Gaussian with $q \simeq 1.935$ is numerically observed in the limiting distribution describing the whole system. This value is expected to converge asymptotically to 2, as we have already seen for the standard map. While this distribution is capable of modeling the entire phase space of the ($p = 1, \epsilon = 0$) system, which is entirely nonergodic, it maintains its

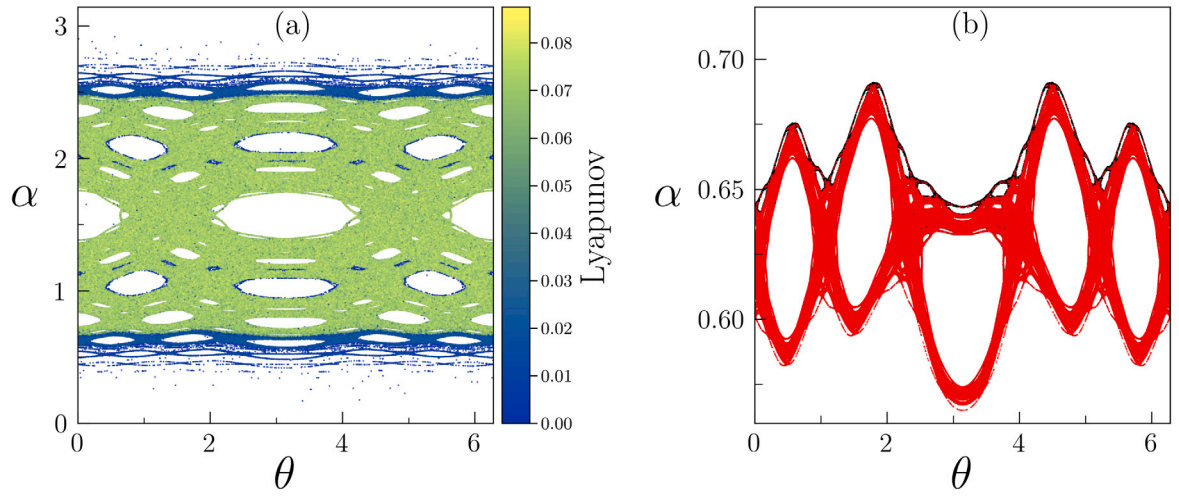

Fig. 3. (a) Lyapunov color map of $p = 1$, $\epsilon = 0.25$ where the stability islands are eliminated. Different chaotic regions can be seen. The observation of sticky behavior is made in the less chaotic region. (b) Sticky region example using two initial condition sets (red color for $[\alpha, \theta] = [0.63, 2.09]$ and black color for $[0.62079, 0.90107]$). Each set is iterated 4×10^5 times. The sticky behavior arising in the phase space causes the contribution of q-Gaussian with $q = 1.25$ in the limiting distribution describing the whole system of $p = 1$, $\epsilon = 0.25$. (For interpretation of the references to color in this figure legend, the reader is referred to the web version of this article.)

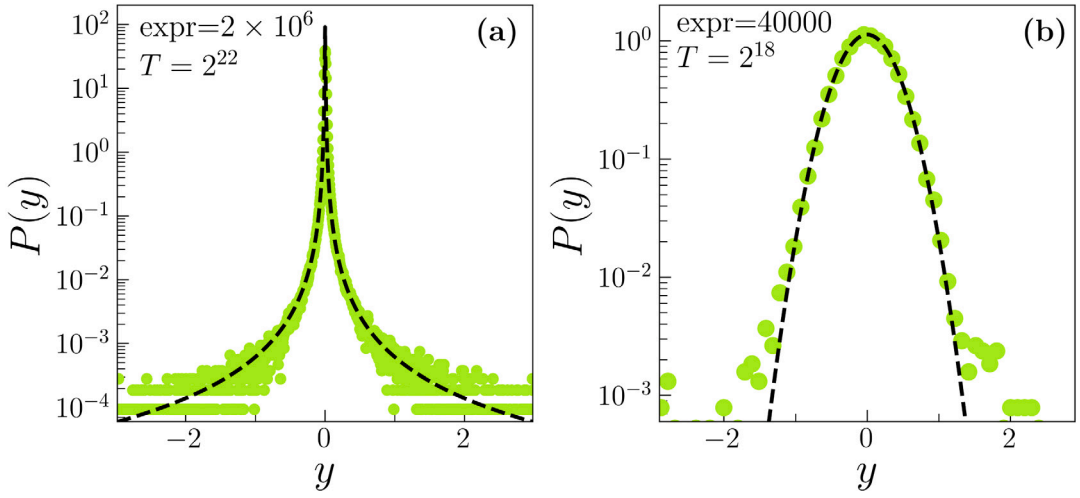

Fig. 4. For the $p = 1$, $\epsilon = 0.25$ case, probability distributions obtained from the initial conditions chosen only from (a) stability islands and (b) chaotic sea. These limiting distributions are maintained together in all scenarios consisting of regular and chaotic behavior and, for the $p = 1$, $\epsilon = 0.25$ case, they are observed with the one resulting from the sticky behavior.

existence together with other distributions in the multicomponent probability distribution for other cases consisting of chaotic sea and stability islands. When the results obtained in this paper are considered together with those of other area-preserving maps mentioned in [7,8,10], one may infer that the consistent observation of a q-Gaussian distribution with an approximate value of $q \simeq 1.935$ for initial conditions residing within the stability islands is a universal phenomenon in numerical analyses of area-preserving systems. In addition, the relationship formed between the sticky behavior and the q-Gaussian distribution is in conformance with the results of [10,11] where it is analyzed and explained in detail. Since the limiting distributions modeling the whole phase space of the selected billiard systems are numerically computed by using a large number of initial conditions, each iterated for long time steps, the limiting distributions presented here are considered to be robust when the finite time constraint and the time requirements of the analyses are taken into consideration. As a future work, one can check whether this tendency also exists for other billiard systems with different boundary definitions.

The results here support the studies demonstrating the use of nonextensive statistical mechanics for such dynamical systems and provide a further link between this statistical mechanical framework and chaos theory. From this point of view, three-dimensional integrable maps, perturbed billiard systems, and quantum billiard systems can be the focus of future theoretical studies. The present work is thought to pave the way for studies that shed light on observations made in experimental and simulation studies. Chaotic billiard lasers [42], microwave billiard systems [43,44], and optical properties of microcavities [45,46] are among the many experimental studies that can be cited as examples.

CRediT authorship contribution statement

Kivanc Cetin: Conceptualization, Data curation, Formal analysis, Investigation, Methodology, Project administration, Validation, Writing – original draft, Writing – review & editing. **Ugur Tirnakli:** Conceptualization, Data curation, Formal analysis, Investigation, Methodology, Project administration, Validation, Writing – original draft, Writing – review & editing. **Diego F.M. Oliveira:** Conceptualization, Formal analysis, Methodology, Validation, Writing – original draft, Writing – review & editing. **Edson D. Leonel:** Conceptualization, Formal analysis, Methodology, Validation, Writing – original draft, Writing – review & editing.

Declaration of competing interest

The authors declare that they have no known competing financial interests or personal relationships that could have appeared to influence the work reported in this paper.

Data availability

Data will be made available on request.

Acknowledgments

The numerical calculations reported in this paper were partially performed at TUBITAK ULAKBIM, High Performance and Grid Computing Center (TRUBA resources). E.D.L. acknowledges support from CNPq (No. 301318/2019-0) and FAPESP (No. 2021/09519-5), Brazilian agencies. U.T. is a member of the Science Academy, Bilim Akademisi, Turkey.

References

[1] Tsallis C. Non-additive entropies and statistical mechanics at the edge of chaos: a bridge between natural and social sciences. Phil Trans R Soc A 2023;381(2256):20220293.
[2] Rodríguez A, Pluchino A, Tirnakli U, Rapisarda A, Tsallis C. Nonextensive footprints in dissipative and conservative dynamical systems. Symmetry 2023;15(2):444.
[3] Tirnakli U, Beck C, Tsallis C. Central limit behavior of deterministic dynamical systems. Phys Rev E 2007;75(4):040106.
[4] Tirnakli U, Tsallis C, Beck C. Closer look at time averages of the logistic map at the edge of chaos. Phys Rev E 2009;79(5):056209.
[5] Cetin K, Afsar O, Tirnakli U. Limit behaviour and scaling relations of two kinds of noisy logistic map in the vicinity of chaos threshold and their robustness. Physica A 2015;424:269–82.
[6] Tirnakli U, Borges EP. The standard map: From Boltzmann-Gibbs statistics to tsallis statistics. Sci Rep 2016;6(1):23644.
[7] Ruiz G, Tirnakli U, Borges EP, Tsallis C. Statistical characterization of the standard map. J Stat Mech 2017;2017(6):063403.
[8] Ruiz G, Tirnakli U, Borges EP, Tsallis C. Statistical characterization of discrete conservative systems: The web map. Phys Rev E 2017;96(4):042158.
[9] Bountis A, Veerman J, Vivaldi F. Cauchy distributions for the integrable standard map. Phys Lett A 2020;384(26):126659.
[10] Tirnakli U, Tsallis C, Cetin K. Dynamical robustness of discrete conservative systems: Harper and generalized standard maps. J Stat Mech 2020;2020(6):063206.
[11] Cetin K, Tirnakli U, Boghosian BM. A generalization of the standard map and its statistical characterization. Sci Rep 2022;12(1):8575.
[12] Berry MV. Regularity and chaos in classical mechanics, illustrated by three deformations of a circular 'billiard'. Eur J Phys 1981;2(2):91.
[13] Chang S-J, Friedberg R. Elliptical billiards and Poncelet's theorem. J Math Phys 1988;29(7):1537–50.
[14] Oliveira DF, Leonel ED. On the dynamical properties of an elliptical–oval billiard with static boundary. Commun Nonlinear Sci 2010;15(4):1092–102.
[15] Oliveira DF, Leonel ED, Robnik M. Boundary crisis and transient in a dissipative relativistic standard map. Phys Lett A 2011;375(38):3365–9.
[16] Oliveira DF, Bizao RA, Leonel ED, et al. Scaling properties of a hybrid Fermi-Ulam-bouncer model. Math Probl Eng 2009;2009.
[17] Oliveira DF, Robnik M, Leonel ED. Statistical properties of a dissipative kicked system: Critical exponents and scaling invariance. Phys Lett A 2012;376(5):723–8.
[18] Sinai YG. Dynamical systems with elastic reflections. Russian Math Surv 1970;25(2):137.
[19] Bunimovich LA. On the ergodic properties of nowhere dispersing billiards. Comm Math Phys 1979;65:295–312.
[20] Chernov N, Eyink G, Lebowitz J, Sinai YG. Steady-state electrical conduction in the periodic Lorentz gas. Comm Math Phys 1993;154:569–601.
[21] Chernov N, Zhang H-K, Zhang P. Electrical current in sinai billiards under general small forces. J Stat Phys 2013;153(6):1065–83.
[22] Tomsovic S, Heller EJ. Long-time semiclassical dynamics of chaos: The stadium billiard. Phys Rev E 1993;47(1):282.
[23] Fermi E. On the origin of the cosmic radiation. Phys Rev 1949;75(8):1169.
[24] Oliveira DF, Leonel ED. In-flight and collisional dissipation as a mechanism to suppress Fermi acceleration in a breathing Lorentz gas. Chaos 2012;22(2).
[25] Blocki J, Boneh Y, Nix J, Randrup J, Robel M, Sierk A, Swiatecki W. One-body dissipation and the super-viscidity of nuclei. Ann Physics 1978;113(2):330–86.
[26] Kobayakawa K, Honda Y, Samura T. Acceleration by oblique shocks at supernova remnants and cosmic ray spectra around the knee region. Phys Rev D 2002;66(8):083004.
[27] Veltri A, Carbone V. Radiative intermittent events during Fermi's stochastic acceleration. Phys Rev Lett 2004;92(14):143901.
[28] Ravnik J, Vaskivskyi Y, Vodeb J, Aupič P, Vaskivskyi I, Golež D, Gerasimenko Y, Kabanov V, Mihailovic D. Quantum billiards with correlated electrons confined in triangular transition metal dichalcogenide monolayer nanostructures. Nature Commun 2021;12(1):3793.
[29] Oliveira DF, Leonel ED. Suppressing Fermi acceleration in a two-dimensional non-integrable time-dependent oval-shaped billiard with inelastic collisions. Physica A 2010;389(5):1009–20.
[30] Hansen M, da Costa DR, Caldas IL, Leonel ED. Statistical properties for an open oval billiard: An investigation of the escaping basins. Chaos Solitons Fractals 2018;106:355–62.
[31] Díaz GI, Palmero MS, Caldas IL, Leonel ED. Diffusion entropy analysis in billiard systems. Phys Rev E 2019;100(4):042207.
[32] Benettin G, Galgani L, Giorgilli A, Strelcyn J-M. Lyapunov characteristic exponents for smooth dynamical systems and for Hamiltonian systems; a method for computing all of them. Part 1: Theory. Meccanica 1980;15:9–20.
[33] Szezech Jr JD, Lopes SR, Viana RL. Finite-time Lyapunov spectrum for chaotic orbits of non-integrable Hamiltonian systems. Phys Lett A 2005;335(5–6):394–401.
[34] Harle M, Feudel U. Hierarchy of islands in conservative systems yields multimodal distributions of FTLEs. Chaos Solitons Fractals 2007;31(1):130–7.
[35] Da Silva R, Manchein C, Beims M, Altmann E. Characterizing weak chaos using time series of Lyapunov exponents. Phys Rev E 2015;91(6):062907.
[36] Artuso R, Manchein C. Instability statistics and mixing rates. Phys Rev E 2009;80(3):036210.
[37] Prato D, Tsallis C. Nonextensive foundation of Lévy distributions. Phys Rev E 1999;60(2):2398.
[38] Birkhoff GD. Nouvelles recherches sur les systèmes dynamiques.... Ex aedibus academicis in Civitate Vaticana; 1934.
[39] Arnold V. Mathematical methods of classical mechanics. New York: Springer-Verlag; 1978.
[40] Contopoulos G, Galgani L, Giorgilli A. On the number of isolating integrals in Hamiltonian systems. Phys Rev A 1978;18(3):1183.
[41] Manchein C, Beims MW, Rost JM. Characterizing the dynamics of higher dimensional nonintegrable conservative systems. Chaos 2012;22(3).
[42] You M, et al. Universal single-mode lasing in fully chaotic billiard lasers. Entropy 2022;24(11):1648.
[43] Carmo Rd, Aguiar Fd. Experimental microwave scattering in polygonal billiards. Sci Rep 2019;9(1):3634.
[44] Dietz B, Richter A. Quantum and wave dynamical chaos in superconducting microwave billiards. Chaos 2015;25(9).
[45] Sunada S, et al. Stable single-wavelength emission from fully chaotic microcavity lasers. Phys Rev A 2013;88(1):013802.
[46] Cao H, Wiersig J. Dielectric microcavities: Model systems for wave chaos and non-hermitian physics. Rev Modern Phys 2015;87(1):61.